Third-Order Nonoscillatory Schemes for the Euler Equations

J. Y. Yang*
National Taiwan University, Taipei, Taiwan 10764, Republic of China

Two time-level third-order finite-difference shock-capturing schemes based on applying the characteristic flux difference splitting to a modified flux that may have high-order accuracy and either monotonicity preserving or essentially nonoscillatory (ENO) property have been developed for the Euler equations of gas dynamics. Two ways to achieve high-order accuracy are described. One is based on upstream interpolation using Lagrange's formula with van Leer's smoothness monitors. The other is based on ENO interpolation using reconstruction via primitive function approaches. For multidimensional problems, dimensional splitting is adopted for explicit schemes, and standard alternating direction implicit approximate factorization procedures are used for implicit schemes. Numerical examples to illustrate the performance of the proposed schemes are given.

I. Introduction

VERY recently, a new class of uniformly high-order accurate, essentially nonoscillatory (ENO) schemes has been developed by Harten and Osher,[1] Harten,[2] and Harten et al.[3,4] They presented a hierarchy of uniformly high-order accurate schemes that generalize Godunov's scheme[5] and its second-order accurate MUSCL extension[6,7] and total variation diminishing (TVD) schemes[8,9] to an arbitrary order of accuracy.

In contrast to the earlier second-order TVD schemes that drop to first-order accuracy at local extrema and maintain second-order accuracy in smooth regions, the new ENO schemes are uniformly high-order accurate throughout, even at critical points.

Theoretical results for the scalar coefficient case and numerical results for the scalar conservation law and for the one-dimensional Euler equations of gas dynamics have been reported with highly accurate results. Preliminary results for two-dimensional problems were reported in Ref. 2.

In this paper, following van Leer,[10,11] Harten,[2] and Harten et al.[3,4] we describe a class of third-order, essentially nonoscillatory shock-capturing schemes for the Euler equations of gas dynamics. These schemes are obtained by applying the characteristic flux-difference splitting to an appropriately modified flux vector that may have high-order accuracy and nonoscillatory property. Third-order schemes are constructed using upstream interpolation and ENO interpolation. Both explicit and implicit schemes are derived. Implicit schemes for two-dimensional Euler equations in general coordinates are also given.

We apply the resulting schemes to simulate one-dimensional and two-dimensional unsteady shock tube flows and steady two-dimensional flows involving strong shocks to illustrate the performance of the schemes. In Sec. II, characteristic properties of the Euler equations related to the numerical advections are briefly summarized.

Upstream interpolation using Lagrange's formula to generate a class of two time-level, $2p+1$ space point, $(2p-1)$th-order accurate schemes is described in Sec. III. In particular, a third-order scheme with smoothness monitors due to van Leer[10] is described.

In Sec. IV, the essentially nonoscillatory interpolation of Harten[2] and Harten et al.[3,4] using reconstruction via primitive function approach is employed to yield a third-order nonoscillatory scheme.

In Sec. V, schemes for two-dimensional Euler equations in general coordinates are outlined. Both explicit schemes for time-dependent problems and implicit schemes for steady-state calculations are given.

Numerical experiments with the proposed third-order schemes for solving several gasdynamic problems are presented in Sec. VI. Conclusions are given in Sec. VII.

II. Euler Equations of Gas Dynamics

Consider the one-dimensional Euler equations of inviscid gasdynamics in conservation law form

$$\partial_t Q + \partial_x F(Q) = 0 \tag{1}$$

where $Q = (\rho, \rho u, e)^T$ is the conservative state vector and $F = [\rho u, \rho u^2 + p, u(e+p)]^T$ the flux vector. Here ρ is the fluid density, u the fluid velocity, p the fluid pressure, and e the total internal energy. For a perfect gas, the pressure is related to other fluid properties by the equation of state $p = (\gamma - 1)(e - \rho u^2/2)$, where γ is the ratio of specific heats.

Equation (1) can be expressed in quasilinear form as

$$\partial_t Q + A(Q)\partial_x Q = 0 \tag{2}$$

where A is the Jacobian matrix $\partial F/\partial Q$. Due to the hyperbolicity of Eq. (1), flux Jacobian matrix A has real eigenvalues

$$a_1 = u, \quad a_2 = u + c, \quad a_3 = u - c \tag{3}$$

where $c = \sqrt{\gamma p/\rho}$ is the sound speed. The corresponding right eigenvectors are

$$r_1(Q) = \left[1, u, \frac{u^2}{2}\right]^T, \qquad r_2(Q) = \frac{\rho}{2c}[1, u + c, H + uc]^T$$

$$r_3(Q) = -\frac{\rho}{2c}[1, u - c, H - uc]^T \tag{4}$$

Here $H = (e+p)/\rho = c^2/(\gamma - 1) + \frac{1}{2}u^2$ is the enthalpy. We first form the matrix T, the columns of which are right eigenvectors in Eq. (4)

$$T(Q) = [r_1(Q), r_2(Q), r_3(Q)]$$

and then define $l_k(Q)$ to be the kth row in T^{-1}, the inverse of $T(Q)$. We have

$$l_1(Q) = \left[1 - (\gamma - 1)\frac{u^2}{2c^2}, (\gamma - 1)\frac{u}{c^2}, -(\gamma - 1)\frac{1}{c^2}\right]$$

$$l_2(Q) = \frac{1}{\rho c}\left[(\gamma - 1)\frac{u^2}{2} - uc, c - (\gamma - 1)u, (\gamma - 1)\right]$$

$$l_3(Q) = \frac{1}{\rho c}\left[(\gamma - 1)\frac{u^2}{2}, c - (\gamma - 1)u, (\gamma - 1)\right] \tag{5}$$

Presented as Paper 90-0110 at the AIAA 28th Aerospace Sciences Meeting, Reno, NV, Jan. 8-11, 1990; received Jan. 30, 1990; revision received Sept. 10, 1990; accepted for publication Sept. 24, 1990.

*Associate Professor, Institute of Applied Mechanics. Member AIAA.

It then follows that

$$A = T\Lambda T^{-1}, \qquad \Lambda = \text{diag}\{a_1\} \tag{6}$$

and Eq. (2) can be put in the following characteristic form:

$$T^{-1}\partial_t Q + \Lambda T^{-1}\partial_x Q = 0 \tag{7}$$

For the purpose of analysis, we assume that the coefficient matrix A is "frozen," that is, constant. By virtue of Eqs. (6) and (7), one can define a characteristic variable $V = (v_1, v_2, v_3)^T = T^{-1}Q$ and transform Eq. (7) to the uncoupled system:

$$\partial_t v_l + a_l \partial_x v_l = 0, \qquad l = 1,2,3 \tag{8}$$

and

$$dv_l = 0 \quad \text{along} \quad \frac{dx}{dt} = a_l \tag{9}$$

Define a uniform computational mesh $\{x_j, t^n\}$, with mesh size Δx and Δt. The discrete representation of $v(x,t)$ on the mesh is v_j^n, and $\lambda = \Delta x/\Delta t$ is the mesh ratio. Suppose that the values v_j^n at time level $t = n\Delta t$ are known and we want to calculate new values at time level $t = (n+1)\Delta t$.

In Fig. 1, leaving point P at (x_j, t^{n+1}), one can draw three curves and intersect line $t = n\Delta t$ at P_0, P_+, and P_- and

$$j\Delta x - x(P_l) = a_l \Delta t \tag{10}$$

$$v_{l,j}^{n+1} - v_l^n(P_l) = 0 \tag{11}$$

Define the Courant number

$$\sigma_l = a_l \Delta t/\Delta x \tag{12}$$

then

$$x(P_l) = (j - \sigma_l)\Delta x \tag{13}$$

$$v_{l,j}^{n+1} = v_{l,j-\sigma_l}^n \tag{14}$$

where $v_{l,j-\sigma_l}^n$ is an approximation for $v_l[(j-\sigma_l)\Delta x, n\Delta t]$.

Equation (14) merely expresses the fact that v_l is invariant along its characteristics, i.e., Eq. (9). Since the values of $v_{j-\sigma_l}$ are not given, one must express it in terms of known values given at the nodal points by some interpolation. Also, the locations of points P_l are determined by their characteristics; this kind of interpolation is upwind biased and is generally referred to as upstream interpolation. It is also noted that depending on the number of nodal points (stencil) used, arbitrary high order of accuracy can be achieved.

III. Upstream Interpolation and Numerical Advections

In the present section, Lagrange's interpolation formula is employed to generate a class of explicit two time-level, $2p+1$ space-point, $(2p-1)$th-order accurate conservative upwind schemes. For simplicity, we drop the index l and consider single equation

$$v_j^{n+1} = v_{j-\sigma}^n \tag{15}$$

Using Lagrange's interpolation formula with equal points on each side of point $j - \sigma$ (see Fig. 2), we have

$$v_{j-\sigma}^n = \sum_{m=-p+1}^{p} \prod_{\substack{i=-p+1 \\ i\neq m}}^{p} \frac{(i - \sigma + [\sigma])}{(i-m)} v_{j-[\sigma]-m}^n \tag{16}$$

Here $[\sigma]$ is the largest integer not exceeding σ. The class of schemes defined by Eq. (16) are stable for

$$|\sigma| \le 1 \tag{17}$$

For $0 \le \sigma \le 1$, $[\sigma] = 0$, and for $-1 \le \sigma \le 0$, $[\sigma] = -1$. (See Ref. 12 and the references cited there.)

For example, for $p = 1$, i.e., we approximate $v_{j-\sigma}^n$ by linear interpolation along the line $t = n\Delta t$, then we have the first-order scheme

$$v_j^{n+1} = v_{j-\sigma}^n = v_{j-[\sigma]}^n - (\sigma - [\sigma])(v_{j-[\sigma]}^n - v_{j-[\sigma]-1}^n) \tag{18}$$

For $|\sigma| \le 1$ this becomes the Courant-Isaacson-Rees method[13]

$$v_j^{n+1} = v_j^n - \lambda a^+ \Delta_- v_j^n - \lambda a^- \Delta_+ v_j^n \tag{19}$$

where

$$a^+ = \frac{(a + |a|)}{2} = \max(a,0)$$

$$a^- = \frac{(a - |a|)}{2} = \min(a,0) \tag{20}$$

and

$$\Delta_\pm v_j^n = \pm(v_{j\pm1}^n - v_j^n)$$

For system Eq. (2), this is easily generalized to

$$Q_j^{n+1} = Q_j^n - \lambda A_{j-\frac{1}{2}}^+ \Delta_- Q_j^n - \lambda A_{j+\frac{1}{2}}^- \Delta_+ Q_j^n \tag{21}$$

where

$$A^\pm = T\,\text{diag}\,(a_l^\pm)T^{-1} \tag{22}$$

Several schemes constructed based on Eq. (21) with shock fitting can be found in a recent review given by Moretti.[14]

If Roe's average is employed to compute $A_{j+\frac{1}{2}}^\pm$, then one has the Roe scheme.[15] Similarly, for the Eq. (1)

$$Q_j^{n+1} = Q_j^n - \lambda \hat{A}_{j-\frac{1}{2}}^+ \Delta_- F_j^n - \hat{A}_{j+\frac{1}{2}}^- \Delta_+ F_j^n \tag{23}$$

where

$$\hat{A}^\pm = T\,\text{diag}(\hat{a}_l^\pm)T^{-1}, \quad \hat{a}_l^\pm = \tfrac{1}{2}(1 \pm \text{sgn}\,a_l) \tag{24}$$

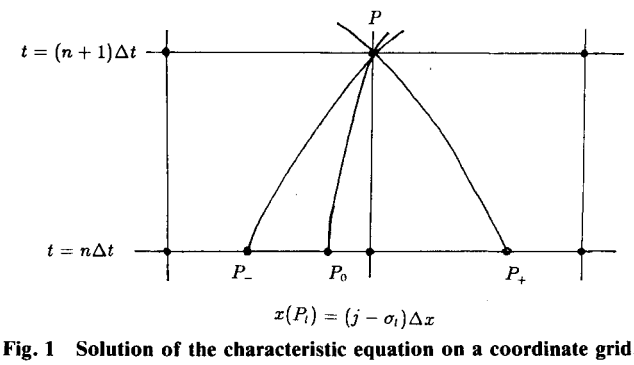

Fig. 1 Solution of the characteristic equation on a coordinate grid.

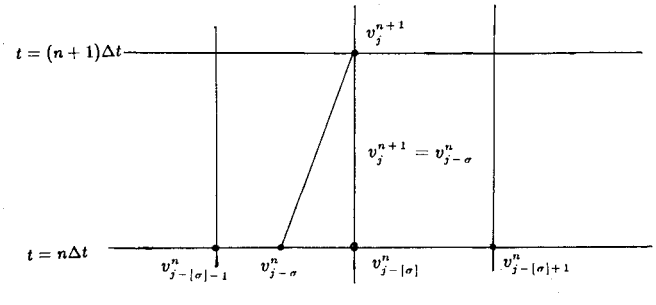

Fig. 2 Upstream interpolation.

The scheme defined by Eq. (29) can be considered as the first-order upwind method for the following:

$$\partial_t Q + (\hat{A}^+ + \hat{A}^-)\partial_x F(Q) = 0 \tag{25}$$

It is noted that $\hat{A}^+ + \hat{A}^- = I$ and symbolically $\hat{A}^\pm$ can be viewed as "$A^\pm/A$."

For pseudo-unsteady Euler equations, the scheme defined by Eq. (23) turns out to be identical to the first-order upwind scheme given by Huang.[16]

For $p = 2$, Eq. (16) becomes

$$\begin{aligned} v_j^{n+1} = v_j^n &- \frac{\sigma - [\sigma]}{6}[2(v_{j-[\sigma]+1}^n - v_{j-[\sigma]}^n) + 5(v_{j-[\sigma]}^n - v_{j-|\sigma|-1}^n) \\ &- (v_{j-[\sigma]-1}^n - v_{j-[\sigma]-2}^n)] \\ &+ \frac{(\sigma - [\sigma])^2}{6}[3(v_{j-[\sigma]+1}^n - v_{j-[\sigma]}^n) - 3(v_{j-[\sigma]}^n - v_{j-[\sigma]-1}^n)] \\ &- \frac{(\sigma - [\sigma])^3}{6}[(v_{j-[\sigma]+1}^n - v_{j-|\sigma|}^n) - 2(v_{j-|\sigma|}^n - v_{j-[\sigma]-1}^n) \\ &+ (v_{j-[\sigma]-1}^n - v_{j-[\sigma]-2}^n)] \end{aligned} \tag{26}$$

which for $|\sigma| \le 1$ is the "QUICKEST" method of Leonard.[17]

For the purpose of the present framework, we further put Eq. (26) into the following form:

$$\begin{aligned} v_j^{n+1} &= v_j^n - (\sigma - [\sigma])\Delta_- v_{j-[\sigma]}^n \\ &- \frac{(\sigma - [\sigma])}{6}\Delta_-\{[2 - 3(\sigma - [\sigma]) + (\sigma - [\sigma])^2]\Delta_+ v_{j-[\sigma]}^n \\ &+ [1 - (\sigma - [\sigma])^2]\Delta_+ v_{j-[\sigma]-1}^n\} \end{aligned} \tag{27}$$

Following the same procedure and using high-order interpolation formula, we can generate a class of high-order accurate, conservative schemes for Eq. (1). Unfortunately, it is well known that oscillatory solutions are usually obtained and eventually lead to numerical instability. Artificial viscosity is generally introduced to a high-order scheme to yield stable solutions.

In recent years, total variation diminishing schemes using flux limiters have been devised for second-order schemes to control such oscillations and yield sharp profiles around discontinuities. Such schemes include van Leer's MUSCL scheme, Harten's TVD schemes, and others. A systematic study has been carried out in Ref. 18. The TVD schemes are high-order accurate everywhere except at local extrema where they necessarily degenerate into first-order accuracy (see Refs. 6, 8, 9, and 15).

In Ref. 19, second- and third-order upwind schemes have been described based on Eq. (16). It was found that such high-order schemes can be constructed for Eq. (25) by using a more accurate flux representation (in the discrete sense) at each nodal point. We have taken such an approach following Harten's work[8] in which he applied a three-point first-order upwind scheme to a modified flux to yield a second-order TVD scheme. Therefore we call it the modified flux approach.

We consider a high-order extension of Eq. (25) as follows:

$$\partial_t Q + (\hat{A}^+ + \hat{A}^-)\partial_x F^M(Q) = 0 \tag{28}$$

Here F_j^M is called the modified flux vector at nodal point j and is consisted of the original flux vector F_j and additional terms of high-order accuracy that usually have some nonlinear control terms to avoid oscillatory solutions. We shall describe several such modified flux vectors to yield different nonoscillatory high-resolution shock-capturing schemes based on Eq. (28).

In terms of numerical flux, a conservative scheme for Eq. (28) can be expressed as

$$Q_j^{n+1} = Q_j^n - \lambda[F_{j+\frac{1}{2}}^N - F_{j-\frac{1}{2}}^N] \tag{29}$$

and the numerical flux $F_{j+\frac{1}{2}}^N$ is given by

$$F_{j+\frac{1}{2}}^N = F_{j+1}^M - \hat{A}_{j+\frac{1}{2}}^+\Delta_+ F_j^M = F_j^M + \hat{A}_{j+\frac{1}{2}}^-\Delta_+ F_j^M \tag{30}$$

In this paper all schemes will be given in the form of Eq. (30) with appropriate definition of F^M for each scheme. We shall consider third-order total variation diminishing and essentially nonoscillatory schemes and term them as TVD3 and UNO3, depending on the type of nonlinear limiters used.

A third-order scheme for Eq. (28) based on Eq. (27) can be expressed in terms of numerical flux of the form Eq. (30) with

$$F_j^M = F_j^{\text{TVD3}} = F_j^n + D_j^n \tag{31}$$

The components of D_j are given by

$$d_j^l = [1 - S(\theta_j^l)]\tilde{d}_{j+\frac{1}{2}}^l + [1 + S(\theta_j^l)]\bar{d}_{j-\frac{1}{2}}^l \tag{32}$$

where $\tilde{d}_{j+\frac{1}{2}}^l$ and $\bar{d}_{j+\frac{1}{2}}^l$ are components of $\tilde{D}_{j+\frac{1}{2}}$ and $\bar{D}_{j+\frac{1}{2}}$ given, respectively, by

$$\tilde{D}_{j+\frac{1}{2}} = \operatorname{sgn} A_{j+\frac{1}{2}}(\lambda^2|A_{j+\frac{1}{2}}|^2 - 3\lambda|A_{j+\frac{1}{2}}| + 2I)\Delta_+ F_j/6 \tag{33}$$

$$\bar{D}_{j+\frac{1}{2}} = \operatorname{sgn} A_{j+\frac{1}{2}}(I - \lambda^2|A_{j+\frac{1}{2}}|^2)\Delta_+ F_j/6 \tag{34}$$

and $S(\theta_j^l)$ is the smoothness monitor given by van Leer[10] as

$$\begin{aligned} S(\theta_j^l) &= 0, \quad \text{if} \quad |\Delta_+ q_j^l| + |\Delta_- q_j^l| = 0 \\ &= \frac{|\Delta_+ q_j^l| - |\Delta_- q_j^l|}{|\Delta_+ q_j^l| + |\Delta_- q_j^l|}, \quad \text{otherwise} \end{aligned} \tag{35}$$

where q_j^l are components of the conservative state vector Q_j.

Without smoothness monitors and for the scalar wave equation, schemes defined by Eq. (31) reduce to Eq. (27). We refer to the schemes defined by Eq. (31) as TVD3.

It is noted that in the present framework the difference operators are always operated on flux vector F instead of the conservative state vector Q such as Eqs. (33) and (34). It is well known that F is a function one order smoother than that of Q for the Euler equations, e.g., across a shock, F is continuous and Q is discontinuous.

IV. Essentially Nonoscillatory Schemes

Most recently, Harten and Osher[1] introduced a new class of nonoscillatory schemes that are of uniformly high-order accuracy. Unlike TVD schemes, nonoscillatory schemes are not required to damp the values of each local extremum at every single time step but are allowed to occasionally accentuate a local extremum.

The design involves an essentially nonoscillatory piecework polynomial reconstruction of the solution from its cell averages, time evolution through an approximate solution of the resulting initial value problem, and averaging of this approximate solution over each cell. For further details, the reader is encouraged to read the original papers, Refs. 1-4.

Essentially Nonoscillatory Interpolation

For illustration purposes, we first consider the following scalar wave equation:

$$\partial_t u + a\partial_x u = 0, \; a > 0 \tag{36}$$

Using reconstruction via the primitive function (RP) approach and for $N = 3$, one has a numerical scheme

$$v_j^{n+1} = v_j^n - \sigma\Delta_- v_j^n - \sigma\Delta_-\left[\left(\frac{1-\sigma}{2}\right)m(\Delta_- v_j^n, \Delta_+ v_j^n)\right] - \sigma\Delta_-\left[\frac{(2-3\sigma+\sigma^2)}{6}\bar{m}(\Delta_-\Delta_- v_j^n, \Delta_-\Delta_+ v_j^n)\right] \quad \text{if} \quad |\Delta_- v_j^n| \le |\Delta_+ v_j^n|$$

$$- \sigma\Delta_-\left[\frac{(\sigma^2-1)}{6}\bar{m}(\Delta_-\Delta_+ v_j^n, \Delta_+\Delta_+ v_j^n)\right] \quad \text{if} \quad |\Delta_- v_j^n| > |\Delta_+ v_j^n| \tag{37}$$

For the purposes of the present framework, one can further put Eq. (37) into the following form:

$$v_j^{n+1} = v_j^n - \sigma\Delta_- v_j^n - \sigma\Delta_-\left\{m\left[\left(\frac{1-\sigma}{2}\right)\Delta_- v_j^n, \left(\frac{1-\sigma}{2}\right)\Delta_+ v_j^n\right] - \sigma\Delta_-\bar{m}\left[\Delta_-\left(\frac{2-3\sigma+\sigma^2}{6}\right)\Delta_- v_j^n, \Delta_-\left(\frac{2-3\sigma+\sigma^2}{6}\right)\Delta_+ v_j^n\right]\right\} \quad \text{if} \quad |\Delta_- v_j^n| \le |\Delta_+ v_j^n|$$

$$- \sigma\Delta_-\bar{m}\left[\Delta_-\left(\frac{\sigma^2-1}{6}\right)\Delta_+ v_j^n, \Delta_+\left(\frac{\sigma^2-1}{6}\right)\Delta_+ v_j^n\right] \quad \text{if} \quad |\Delta_- v_j^n| > |\Delta_+ v_j^n| \tag{38}$$

In Eq. (37), m is the minmod function defined by

$$m(a,b) = s\min(|a|,|b|), \quad \text{if} \quad \text{sgn}a = \text{sgn}b = s$$
$$= 0, \quad \text{otherwise} \tag{39}$$

and $\bar{m}$ function is defined by

$$\bar{m}(a,b) = a, \quad \text{if} \quad |a| \le |b|$$
$$= b, \quad \text{if} \quad |a| > |b| \tag{40}$$

Again, we have quantities like $(2-3\sigma+\sigma^2)\Delta_- v_j^n/6$ and $(\sigma^2-1)\Delta_- v_j^n/6$ as the building elements, and the limiting functions are operating on such quantities. The generalization to nonlinear systems is rather straightforward.

A third-order ENO scheme for Eq. (28) can be constructed using RP and $N = 3$ based on Eq. (38). Here

$$F_j^M = F_j^{\text{UNO3}} = F_j + E_j + D_j \tag{41}$$

and E and D are the terms that make up for the higher order accuracy that also demands either the TVD or the ENO property to avoid Gibbs phenomena.

In Eq. (41) the components of column vector E_j are given by

$$e_j^l = m[\tilde{e}_{j+\frac{1}{2}}^l, \tilde{e}_{j-\frac{1}{2}}^l] \tag{42}$$

where $\tilde{e}_{j+\frac{1}{2}}^l$ are given by

$$\tilde{E}_{j+\frac{1}{2}} = \text{sgn}A_{j+\frac{1}{2}}(I - \lambda|A|)\Delta_+ F_j/2 \tag{43}$$

And the components of column vector D_j are given by

$$d_j^l = m[\Delta_-\tilde{d}_{j-\frac{1}{2}}^l, \Delta_+\tilde{d}_{j-\frac{1}{2}}^l] \quad \text{if} \quad |\Delta_{j-\frac{1}{2}}q^1| \le |\Delta_{j+\frac{1}{2}}q^1| \tag{44a}$$

or

$$d_j^l = m[\Delta_-\hat{d}_{j+\frac{1}{2}}^l, \Delta_+\hat{d}_{j+\frac{1}{2}}^l] \quad \text{if} \quad |\Delta_{j-\frac{1}{2}}q^1| > |\Delta_{j+\frac{1}{2}}q^1| \tag{44b}$$

where $\tilde{d}_{j+\frac{1}{2}}^l$ and $\hat{d}_{j+\frac{1}{2}}^l$ are components of $\tilde{D}_{j+\frac{1}{2}}$ and $\hat{D}_{j+\frac{1}{2}}$, respectively.

$\tilde{D}$ is given by Eq. (33) and $\hat{D}$ is given by

$$\hat{D}_{j+\frac{1}{2}} = \text{sgn}A_{j+\frac{1}{2}}(\lambda^2|A_{j+\frac{1}{2}}|^2 - I)\Delta_+ F_j/6 \tag{45}$$

The relationship between Eq. (41) and the scheme defined by Eq. (37) can be clearly seen by examining the scalar constant coefficient case of Eq. (36).

V. Euler Equations in General Coordinates

We consider the conservation equations of the two-dimensional unsteady gasdynamics in general coordinates (ξ,η)

$$\partial_\tau Q + \partial_\xi F + \partial_\eta G = 0 \tag{46}$$

where $Q = \hat{Q}/J, F = (\xi_t\hat{Q} + \xi_x\hat{F} + \xi_y\hat{G})/J$; $G = (\eta_t\hat{Q} + \eta_x\hat{F} + \eta_y\hat{G})/J$; $J = \xi_x\eta_y - \xi_y\eta_x$, the metric Jacobian; $\hat{Q} = (\rho, \rho u, \rho v, e)^T$ is the conservative variables vector; and $\hat{F} = [\rho u, \rho u^2 + p, \rho uv, u(e+p)]^T$ and $\hat{G} = [\rho v, \rho uv, \rho v^2 + p, v(e+p)]^T$ are the flux vectors. Here ρ is the fluid density, u and v are velocity components in x and y direction, e is the total internal energy, and p is the pressure and is related to other variables by $p = (\gamma - 1)[e - \rho(u^2 + v^2)/2]$ where γ is the ratio of specific heats.

The Jacobian coefficient matrices $A_\xi = \partial F/\partial Q$ and $B_\eta = \partial G/\partial Q$ of the transformed equations have real eigenvalues

$$a_1 = U, \; a_2 = U + c_\xi, \; a_3 = U, \; a_4 = U - c_\xi$$

$$b_1 = V, \; b_2 = V, \; b_3 = V + c_\eta, \; b_4 = V - c_\eta$$

with $U = \xi_t + \xi_x u + \xi_y v$, $V = \eta_t + \eta_x u + \eta_y v$, and $c_\xi = c\sqrt{\xi_x^2 + \xi_y^2}$, where $c = \sqrt{\gamma p/\rho}$ is the speed of sound.

One can also find similarity transformation matrices T_ξ and $T\eta$ that diagonize A_ξ and B_η

$$T_\xi^{-1}A_\xi T_\xi = \Lambda_\xi = \text{diag}\{a_l\}, \quad T_\eta^{-1}B_\eta T_\eta = \Lambda_\eta = \text{diag}\{b_l\}$$

Similar to the one-dimensional case given before, we have

$$\partial_\tau Q + (\hat{A}_\xi^+ + \hat{A}_\xi^-)\partial_\xi F^M + (\hat{B}_\eta^+ + \hat{B}_\eta^-)\partial_\eta G^M = 0 \tag{47}$$

where $\hat{A}_\xi^\pm$ and $\hat{B}_\eta^\pm$ are the split normalized Jacobian coefficient matrices. They are given by

$$T_\xi^{-1}\hat{A}^\pm T_\xi = \hat{\Lambda}_\xi^\pm = \text{diag}\{\hat{a}_l^\pm\}, \quad \hat{a}_l^\pm = \tfrac{1}{2}(1 \pm \text{sgn}a_l) \tag{48a}$$

$$T_\eta^{-1}\hat{B}^\pm T_\eta = \hat{\Lambda}_\eta^\pm = \text{diag}\{\hat{b}_l^\pm\}, \quad \hat{b}_l^\pm = \tfrac{1}{2}(1 \pm \text{sgn}b_l) \tag{48b}$$

Again, here $F^M = F + E^\xi + D^\xi$ and $G^M = G + E^\eta + D^\eta$ are modified fluxes. The construction procedure is exactly the same as that for one space dimension.

Explicit Schemes

Let us define a uniform computational mesh system (ξ_j, η_k) with mesh sizes $\Delta\xi = \Delta\eta = 1$, and let $Q_{j,k}^n$ denote the value of Q at time level $n\Delta\tau$ and at position $(j\Delta\xi, k\Delta\eta)$.

For explicit methods in two space dimensions, the Strang-type dimensional splitting[29] was employed.

$$Q_{j,k}^{n+2} = L_\xi(\Delta\tau)L_\eta(\Delta\tau)L_\eta(\Delta\tau)L_\xi(\Delta\tau)Q_{j,k}^n \tag{49}$$

The one-dimensional L_ξ operator is defined by

$$L_\xi Q^n_{j,k} = Q^n_{j,k} - \Delta\tau(F^N_{j+\frac{1}{2},k} - F^N_{j-\frac{1}{2},k}) \tag{50}$$

with

$$F^N_{j+\frac{1}{2},k} = F^M_{j,k} - \hat{A}^+_{j+\frac{1}{2},k}\Delta_{j+\frac{1}{2},k}F^M_{j,k} \tag{51}$$

A third-order method based on using $N = 3$ in the RP (reconstruction via primitive functions) can be given in the form of Eq. (47), except that the modified flux vectors F^M and G^M are now expressed as

$$F^M_{j,k} = F^n_{j,k} + E^\xi_{j,k} + D^\xi_{j,k} \tag{52a}$$

$$G^M_{j,k} = G^n_{j,k} + E^\eta_{j,k} + D^\eta_{j,k} \tag{52b}$$

In Eqs. (52a) and (52b), $E^\xi_{j,k}$ is the same as Eq. (43), and $D^\xi_{j,k}$ is given the same as Eqs. (44a) and (44b) in Sec. IV with

$$\tilde{D}^\xi_{j+\frac{1}{2},k} = \operatorname{sgn}A_{j+\frac{1}{2},k}(\Delta\tau^2|A|^2 - 3\Delta\tau|A| + 2I)_{j+\frac{1}{2},k}\Delta_{j+\frac{1}{2},k}F/6 \tag{53}$$

$$\bar{D}^\xi_{j+\frac{1}{2},k} = \operatorname{sgn}A_{j+\frac{1}{2},k}(\Delta\tau^2|A_{j+\frac{1}{2},k}|^2 - I)\Delta_{j+\frac{1}{2},k}F/6 \tag{54}$$

The components of column vector $E^\xi_{j,k}$ are given by

$$e_{j,k} = m[\tilde{e}_{j+\frac{1}{2},k}, \tilde{e}_{j-\frac{1}{2},k}] \tag{55}$$

Similar expressions can be given for E^η and D^η in the η direction.

For the explicit third-order scheme in two dimensions, we still employ the dimensional splitting. The numerical simulations given in a later section indicate that such a procedure works well.

Implicit Schemes

Implicit schemes for steady-state calculations can be consistently constructed based on the explicit schemes. Following Refs. 21 and 22, implicit methods using backward Euler in time and approximate factorization can be given for Eq. (47). See also Refs. 23–25.

For the modified flux F^M in the ξ direction, this yields

$$\begin{aligned} F^{M^{n+1}} &= F^{M^n} + \Delta\tau(\partial F^M/\partial\tau)^n + O(\Delta\tau^2) \\ &= F^{M^n} + \Delta\tau(A^M\partial Q/\partial\tau)^n + O(\Delta\tau^2) \\ &= F^{M^n} + A^{M^n}(Q^{n+1} - Q^n) + O(\Delta\tau^2) \end{aligned} \tag{56}$$

where A^M is the modified flux Jacobian defined by $A^M = \partial F^M/\partial Q$.

Similar expressions can be given for G^M in the η direction.

The implicit scheme for Eq. (47) in ADI approximate factorization form is

$$[I + \Delta\tau\hat{A}^+_{j-\frac{1}{2},k}\Delta_- A^M_\xi + \Delta\tau\hat{A}^-_{j+\frac{1}{2},k}\Delta_+ A^M_\xi]\Delta Q^*_{j,k} = RHS_{j,k} \tag{57a}$$

$$[I + \Delta\tau\hat{B}^+_{j,k-\frac{1}{2}}\Delta_- B^M_\eta + \Delta\tau\hat{B}^-_{j,k+\frac{1}{2}}\Delta_+ B^M_\eta]\Delta Q^n_{j,k} = \Delta Q^*_{j,k} \tag{57b}$$

$$Q^{n+1}_{j,k} = Q^n_{j,k} + \Delta Q^n_{j,k} \tag{57c}$$

$$RHS_{j,k} = -\Delta\tau[F^N_{j+\frac{1}{2},k} - F^N_{j-\frac{1}{2},k}] - \Delta\tau[G^N_{j,k+\frac{1}{2}} - G^N_{j,k-\frac{1}{2}}] \tag{58}$$

where the numerical fluxes $F^N_{j+\frac{1}{2},k}$ and $G^N_{j,k+\frac{1}{2}}$ are given previously. The modified Jacobian matrices $A^M_\xi = A_\xi + \partial E^\xi/\partial Q + \partial D^\xi/\partial Q$ and $B^M_\eta = B_\eta + \partial E^\eta/\partial Q + \partial D^\eta/\partial Q$ keep the high-order contribution and make the scheme more diagonally dominant. But in practice, they are difficult to compute analytically. A simplified or linearized version is used, that is,

$$A^M_\xi \approx A_\xi \quad \text{and} \quad B^M_\eta \approx B_\eta \tag{59}$$

Then Eqs. (57a–57c) become

$$[I + \Delta\tau\hat{A}^+_{j-\frac{1}{2},k}\Delta_- A_\xi + \Delta\tau\hat{A}^-_{j+\frac{1}{2},k}\Delta_+ A_\xi]\Delta Q^* = RHS_{j,k} \tag{60a}$$

$$[I + \Delta\tau\hat{B}^+_{j,k-\frac{1}{2}}\Delta_- B_\eta + \Delta\tau\hat{B}^-_{j,k+\frac{1}{2}}\Delta_+ B_\eta]\Delta Q^n = \Delta Q^*_{j,k} \tag{60b}$$

$$Q^{n+1}_{j,k} = Q^n_{j,k} + \Delta Q^n_{j,k} \tag{60c}$$

Both Eqs. (57a–57c) and Eqs. (60a–60c) lead to standard block tridiagonal inversion procedure. In the following, implicit numerical results are obtained using Eqs. (60a–60c).

It is noted that each added high-order term of the right-hand side [e.g., Eq. (53) and Eq. (54)] is a function of the time step $\Delta\tau$, and consequently the steady-state solutions will depend on the time step.

VI. Numerical Results and Discussions

Results of several numerical experiments are given in this section to illustrate some characteristics of the present third-order nonoscillatory schemes as applied to one-dimensional and two-dimensional gasdynamic problems with strong shocks. Both unsteady flow results using explicit schemes and steady-state solutions using implicit schemes are included.

Interaction of Blast Waves

We first present numerical experiments with the preceding two schemes for the problem of two interacting blast waves suggested by Woodward and Colella[26] as a test problem; we refer the reader to Ref. 26 where a comprehensive comparison of the performance of various schemes for this problem is presented. The initial states are given by

$$U(x,0)\begin{cases} = U_L, & 0 \le x < 0.1 \\ = U_M, & 0.1 \le x < 0.9 \\ = U_R, & 0.9 \le x < 1 \end{cases}$$

where

$$\rho_L = \rho_M = \rho_R = 1, \qquad u_L = u_M = u_R = 0$$

$$p_L = 10^3, \qquad p_M = 10^{-2}, \qquad p_R = 10^2$$

For comparison purposes, we also include the results obtained using the second-order schemes TVD2 and ENO2 from Refs. 27 and 25, respectively.

Figures 3–6 indicate the computed solutions (circles) of density obtained using TVD2, TVD3, ENO2, and UNO3 schemes with the modified flux approach. The solid line is the "exact" solution taken from Ref. 26. Using a uniform grid system of $J = 400$ points, the CPU time required for 683 time integrations to reach time $t = 0.038$ is 87.56 s for TVD2 scheme, 106.63 s for TVD3 scheme, 99.5 s for ENO2 scheme, and 158.73 s for UNO3 scheme on a Convex C-1 computer.

Here we have used Eqs. (42) and (43) with both $\bar{m}$ replaced by the minmod function m. Comparing these solutions to the "exact" solution of Woodward and Colella, we find that all the important features of the various interactions were captured. The ENO results represent the three contact discontinuities better than the TVD results do.

Shock Wave Reflection by a Circular Cylinder

In this problem we consider a plane shock wave located initially at a certain distance ahead of the circular cylinder that propagates with shock Mach number $M_s = 2.81$ toward the

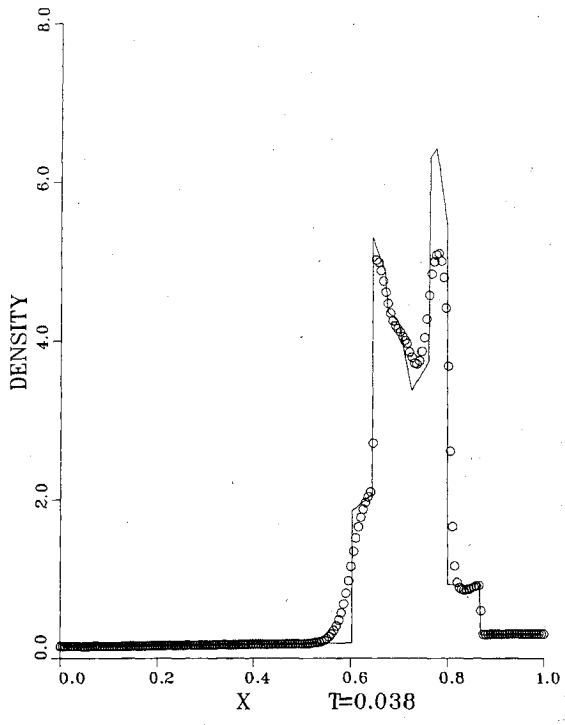

Fig. 3 Solution of one-dimensional interacting blast waves, TVD2 scheme.

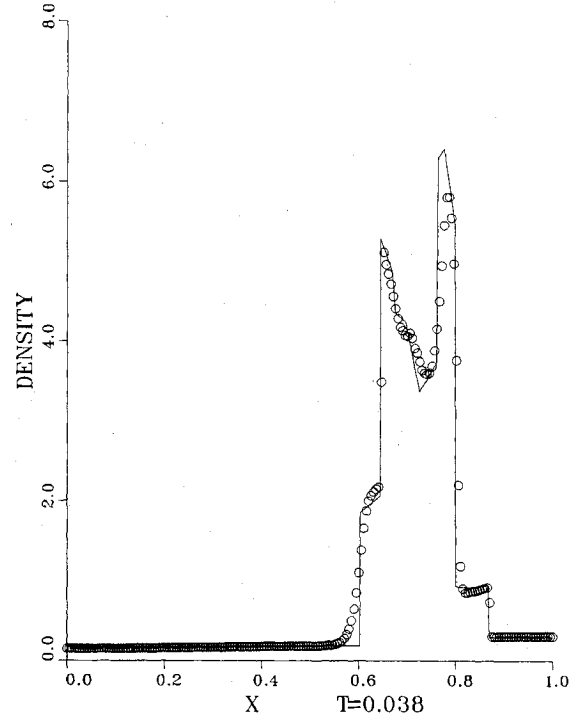

Fig. 4 Solution of one-dimensional interacting blast waves, ENO2 scheme.

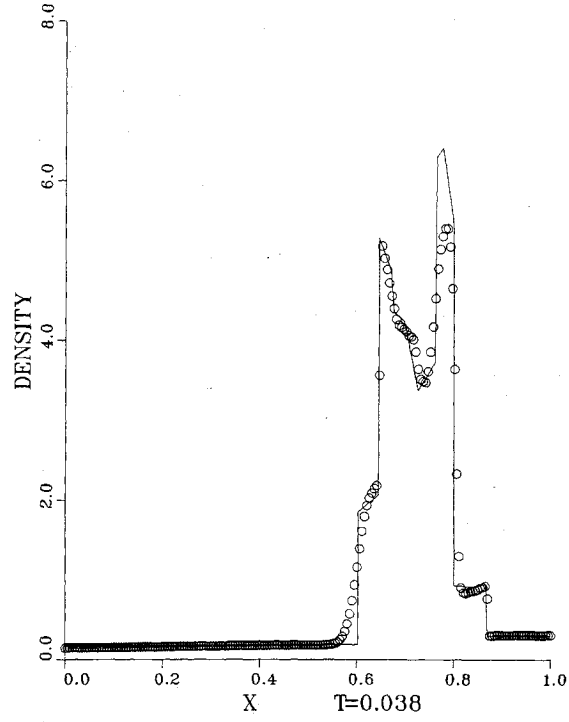

Fig. 5 Solution of one-dimensional interacting blast waves, TVD3 scheme.

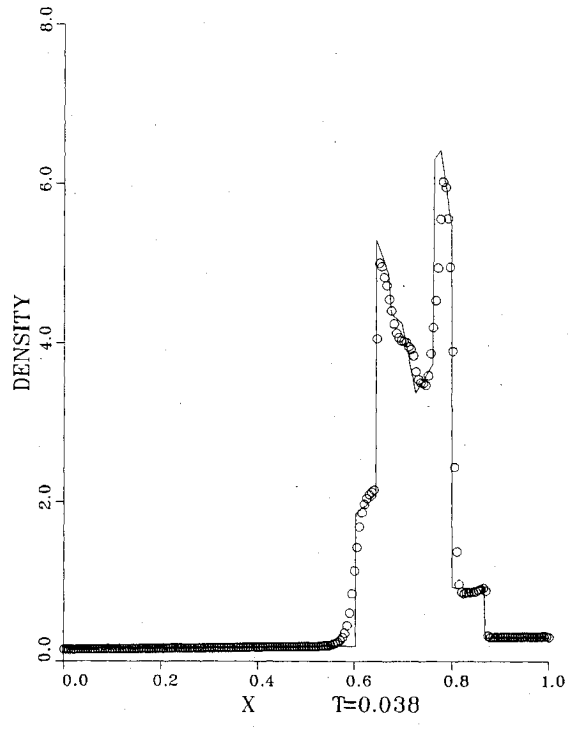

Fig. 6 Solution of one-dimensional interacting blast waves, UNO3 scheme.

cylinder and experiences truly nonstationary shock reflection. A detailed study of this problem using TVD2 and ENO2 schemes has been given in Refs. 27 and 25, respectively. Here only the UNO3 results are reported. A grid system of 361×101 was used. For the UNO3 scheme, we still employed Eq. (49), although it was only proved for second-order accurate schemes in Ref. 20. In Fig. 7, the density and Mach number contours obtained using UNO3 at some instant are shown for a shock Mach number $M_s = 2.81$. A comparison with an experimental schlieren picture has been made in Ref. 27 and will not be repeated here. Excellent agreement is found in nearly every aspect, except for some viscous effects not accounted for by the Euler equations.

The aforementioned numerical experiments demonstrate the capability of the present explicit ENO scheme for time-dependent problems; the quality is quite good. Next we consider a steady-state aerodynamic problem using the implicit ENO scheme.

Transonic Flow over a Circular Arc

We consider an internal two-dimensional transonic flow through a parallel channel having a 4.2% thick circular arc at

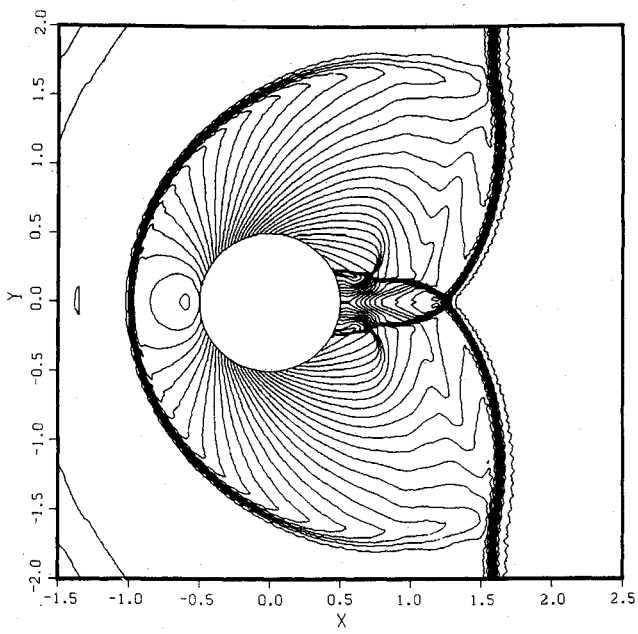

a) Density contours

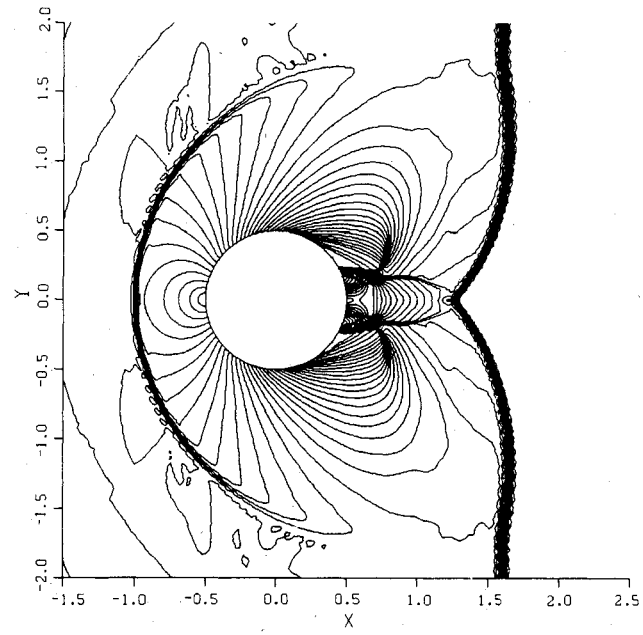

b) Mach number contours

Fig. 7 Computed solution by UNO3 for shock reflection by a cylinder at $M_s = 2.81$.

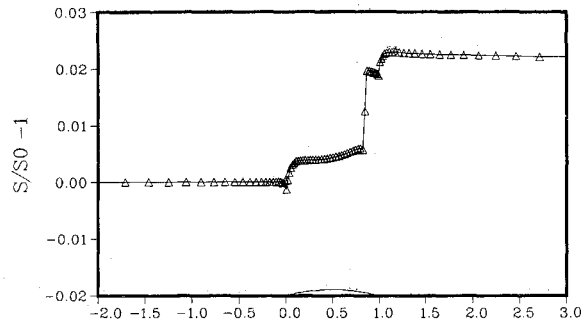

a) Entropy distribution

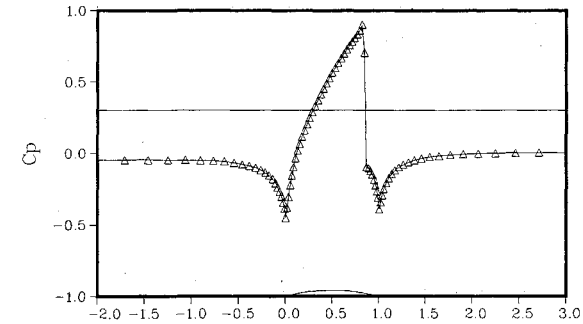

b) C_p distribution

Fig. 8 Solution of transonic channel flow, TVD2 scheme.

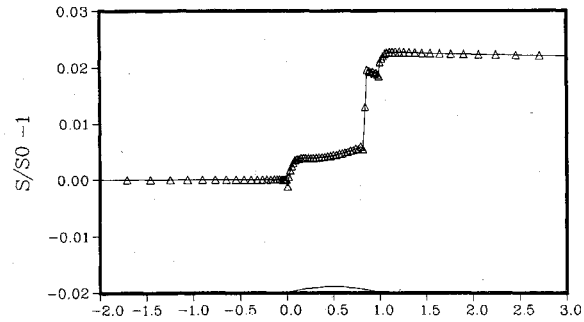

a) Entropy distribution

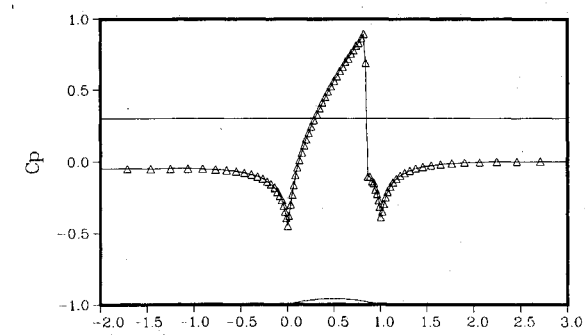

b) C_p distribution

Fig. 9 Solution of transonic channel flow, ENO2 scheme.

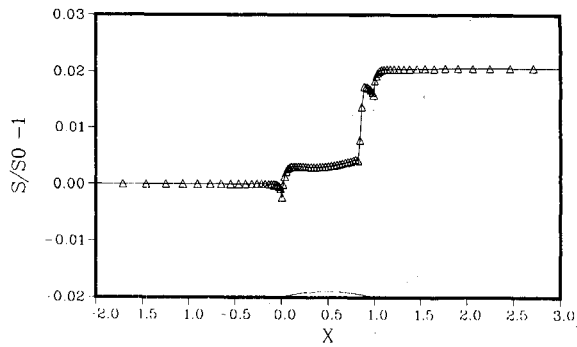

a) Entropy distribution

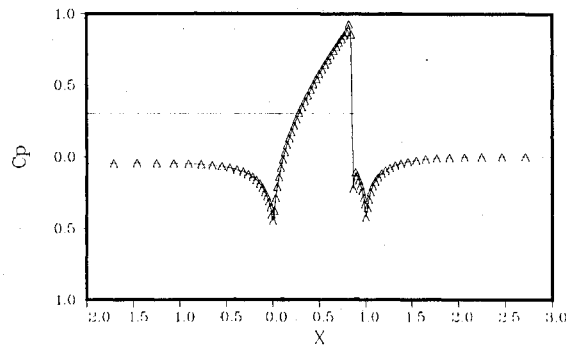

b) C_p distribution

Fig. 10 Solution of transonic channel flow, UNO3 scheme.

the lower wall. The ratio of static downstream pressure to total pressure is 0.623512, corresponding to $M_\infty = 0.85$ in the isentropic flow. In Figs. 8, 9, and 10, the entropy and the C_p distributions at the lower surface for the alternating direction implicit solution with TVD2, ENO2, and UNO3 schemes are shown. It is noted that all three schemes achieve almost the same quality of results. The TVD2 and ENO2 results were computed with Courant-Friedrichs-Lewy (CFL) number 7 for 600 steps, and the ENO3 results were obtained with CFL = 4 for 1050 steps. The lower Courant number used for UNO3 may be attributed to the dependence on the time step.

For the 85×21 grid system used, the CPU time required for the TVD2 implicit methods is 1.026 s per step on a Convex C-1 computer, and it takes 1.043 s for the ENO2 scheme and 1.13 s for the UNO3 scheme.

VII. Concluding Remarks

Two third-order (both in time and space) accurate nonoscillatory shock-capturing schemes have been developed for the Euler equations. The schemes are obtained by applying the first-order characteristic flux difference splitting scheme to an appropriately modified flux vector. Both upstream interpolation and ENO interpolation were employed. When there is no limiting mechanism, the upstream interpolation using Lagrange's formula and ENO interpolation using Newton divided difference to yield high-order accuracy show very similar nature. The upstream interpolation uses Lax-Wendroff type expansion procedure, but the ENO interpolation intrinsically uses a moving stencil and hence has a very different underlying design principle. Implicit schemes are also described for two-dimensional Euler equations in general curvilinear coordinates. Numerical results from steady and unsteady gasdynamical problems with strong shocks demonstrate their robust stability and high resolution of flowfields. We recommend the explicit UNO3 scheme for simulating time-dependent problems. Further improvement to remove the time-step dependence of the steady-state solutions of the present implicit scheme is warranted.

Acknowledgments

This work has been supported by the National Science Council of the Republic of China under Contract NSC 78-0210-D002-11. The author thanks Chang-An Hsu and B. S. Fung for carrying out some of the calculations reported here. Many valuable comments and suggestions from the reviewers are also gratefully acknowledged.

References

[1]Harten, A., and Osher, S., "Uniformly High-Order Accurate Nonoscillatory Schemes I," *SIAM Journal on Numerical Analysis,* Vol. 24, No. 2, 1987, pp. 279–309.

[2]Harten, A., "Preliminary Results on the Extension of ENO Schemes to Two-Dimensional Problems," *Proceedings of the International Conference on Hyperbolic Problems*, Saint-Etienne, France, Jan. 1986.

[3]Harten, A., Engquist, B., Osher, S., and Chakravarthy, S. R., "Uniformly High Order Accurate Essentially Non-Oscillatory Schemes III," *Journal of Computational Physics*, Vol. 71, No. 2, 1987, pp. 231–303.

[4]Harten, A., Osher, S., Engquist, B., and Chakravarthy, S. R., "Some Results on Uniformly High Order Accurate Essentially Non-Oscillatory Schemes," *Journal of Applied Numerical Mathematics,* Vol. 2, No. 2, 1986, pp. 347–367.

[5]Godunov, S. K., "A Finite Difference Method for the Numerical Computation of Discontinuous Solutions of the Equations of Fluid Dynamics," *Mat. Sbornik,* Vol. 47, 1959, pp. 271–290; translated as U.S. Dept of Commerce, JPRS 7225, 1960.

[6]Van Leer, B., "Towards the Ultimate Conservative Difference Scheme V, A Second-Order Sequel to Godunov's Method," *Journal of Computational Physics,* Vol. 32, No. 1, 1979, pp. 234–245.

[7]Colella, P., and Woodward, P. R., "The Piecewise Parabolic Method (PPM) for Gas-Dynamical Simulation," *Journal of Computational Physics*, Vol. 54, No. 1, 1984, pp. 174–201.

[8]Harten, A., "High Resolution Schemes for Hyperbolic Conservation Laws," *Journal of Computational Physics,* Vol. 49, No. 2, 1983, pp. 357–393.

[9]Osher, S., and Charkravathy, S. R., "High Resolution Schemes and Entropy Conditions," *SIAM Journal on Numerical Analysis*, Vol. 21, No. 4, 1984, pp. 955–984.

[10]Van Leer, B., "Towards the Ultimate Conservative Difference Scheme II, Monotonicity and Conservation Combined in a Second-Order Scheme," *Journal of Computational Physics,* Vol. 14, No. 2, 1974, pp. 361–370.

[11]Van Leer, B., "Towards the Ultimate Conservative Difference Scheme III, Upstream-Centered Finite-Difference Schemes For Ideal Compressible Flow," *Journal of Computational Physics,* Vol. 23, No. 2, 1977, pp. 263–275.

[12]Niessner, H., "Comparison of Different Numerical Methods for Calculating One-Dimensional Unsteady Flows," Lecture No. 16, Lecture Series 1980-1, von Kármán Institute for Fluid Dynamics, Rohde-Saint-Genese, Belgium, 1981.

[13]Courant, R., Isaacson, E., and Rees, M., "On the Solution of Nonlinear Hyperbolic Differential Equations by Finite Difference," *Communications in Pure and Applied Mathematics.* Vol. 5, 1952, pp. 243–255.

[14]Moretti, G., "Computation of Flows with Shocks," *Annual Review of Fluid Mechanics,* Vol. 19, 1987, pp. 313–337.

[15]Roe, P. L., "Approximate Riemann Solvers, Parameter Vectors, and Difference Schemes," *Journal of Computational Physics*, Vol. 43, No. 2, 1981, pp. 357–372.

[16]Huang, L. C., "Pseudo-Unsteady Difference Schemes for Discontinuous Solutions of Steady-State One-Dimensional Fluid Dynamics Problems," *Journal of Computational Physics*, Vol. 42, No. 1, 1981, pp. 195–211.

[17]Leonard, B. P., "A Stable and Accurate Convective Modelling Procedure Based on Quadratic Upstream Interpolation," *Computer Methods in Applied Mechanics and Engineering*, Vol. 19, No. 1, 1979, pp. 59–98.

[18]Sweby, P. K., "High Resolution Schemes Using Flux Limiters for Hyperbolic Conservation Laws," *SIAM Journal on Numerical Analysis*, Vol. 21, No. 5, 1984, pp. 995–1011.

[19]Yang, J. Y., "Second- and Third-Order Upwind Flux Difference Splitting Schemes for the Euler Equations,"NASA TM-85959, July 1984.

[20]Strang, G., "On the Construction and Comparison of Difference Schemes," *SINUM,* Vol. 5, 1968, pp. 506–517.

[21]Steger, J. L., and Warming, R. F., "Flux Vector Splitting of Inviscid Gasdynamic Equations with Application to Finite Difference Methods," *Journal of Computational Physics,* Vol. 40, No. 2, 1981, pp. 263–293.

[22]Warming, R. F., and Beam, R. M., "An Implicit Finite Difference Algorithm for Hyperbolic Systems in Conservation Law Form," *Journal of Computational Physics,* Vol. 22, No. 1, 1976, pp. 234–245.

[23]Yee, H. C., Warming, R. F., and Harten, A., "Implicit Total Variation Diminishing (TVD) Schemes for Steady-State Calculations," *Journal of Computational Physics,* Vol. 57, 1985, pp. 327–360.

[24]Yee, H. C., and Harten, A., " Implicit TVD Schemes for Hyperbolic Conservation Laws in Curvilinear Coordinates," *AIAA Journal*, Vol. 25, No. 2, 1987, pp. 266–274.

[25]Yang, J. Y., and Lombard, C. K., "Uniformly Second Order Essentially Nonoscillatory Schemes for the Euler Equations," *AIAA Journal,* Vol. 28, No. 12, 1990, pp. 2069–2076.

[26]Woodward, P., and Colella, P., "The Numerical Simulation of Two-Dimensional Fluid Flow With Strong Shocks," *Journal of Computational Physics,* Vol. 54, No. 1, 1984, pp. 115–173.

[27]Yang, J. Y., Lui, Y., and Lomax, H., "Computation of Shock-Wave Reflection by Circular Cylinders," *AIAA Journal*, Vol. 25, No. 5, 1987, pp. 683–689.